Cellular and Molecular Life Sciences (2024) 81:370
https://doi.org/10.1007/s00018-024-05407-9

ORIGINAL ARTICLE

Notch transcriptional target tmtc1 maintains vascular homeostasis

Na Yoon Paik[1] · Jacob Neethling[1] · Mumtaz Anwar[1] · Prerak Gupta[1] · Mark A. Sanborn[2] · Zekun Shen[1] · Thilinie Bandara[1] · James Hyun[1] · L. A. Naiche[3] · Jan K. Kitajewski[3] · Jalees Rehman[2] · Jae-Won Shin[1] · Dolly Mehta[1] · Kostandin V. Pajcini[1]

Received: 17 February 2024 / Revised: 31 July 2024 / Accepted: 11 August 2024

Abstract

Proper lung function requires the maintenance of a tight endothelial barrier while simultaneously permitting the exchange of macromolecules and fluids to underlying tissue. Disruption of this barrier results in an increased vascular permeability in the lungs, leading to acute lung injury. In this study, we set out to determine whether transcriptional targets of Notch signaling function to preserve vascular integrity. We tested the in vivo requirement for Notch transcriptional signaling in maintaining the pulmonary endothelial barrier by using two complementary endothelial-specific Notch loss-of-function murine transgenic models. Notch signaling was blocked using endothelial-specific activation of an inhibitor of Notch transcriptional activation, Dominant Negative Mastermindlike (DNMAML; CDH5Cre^{ERT2}), or endothelial-specific loss of Notch1 (Notch1$^{f/f}$; CDH5Cre^{ERT2}). Both Notch mutants increased vascular permeability with pan-Notch inhibition by DNMAML showing a more severe phenotype in the lungs and in purified endothelial cells. RNA sequencing of primary lung endothelial cells (ECs) identified novel Notch targets, one of which was transmembrane *O*-mannosyltransferase targeting cadherins 1 (tmtc1). We show that tmtc1 interacts with vascular endothelial cadherin (VE-cadherin) and regulates VE-cadherin egress from the endoplasmic reticulum through direct interaction. Our findings demonstrate that Notch signaling maintains endothelial adherens junctions and vascular homeostasis by a transcriptional mechanism that drives expression of critical factors important for processing and transport of VE-cadherin.

Keywords Vascular permeability · Notch signaling · Endothelial cells

Significance statement

We genetically and functionally investigated the role of Notch signaling in lung vascular endothelial adherens junctions. Utilizing two in vivo, inducible, endothelial-specific, loss-of-function transgenic murine models and in vivo small molecule inhibition of Notch signaling by gamma secretase inhibitors, we reveal a critical role for canonical, transcriptional Notch signaling in maintaining endothelial barrier function. We also identify tmtc1 as a novel downstream target of Notch signaling in vascular endothelial cells.

Introduction

A tight vascular endothelial barrier is essential for proper lung function by dynamically regulating the transendothelial exchange of fluid, proteins, and immune cells to the underlying tissue. Endothelial cells (ECs) establish this continuous barrier by forming adherens junctions through the expression and assembly of tight junctional proteins [1–3]. A disruption to this barrier leads to an increased vascular permeability in the lungs, causing edema and neutrophilic inflammation, a hallmark of acute lung injury (ALI) and its severe form, acute respiratory distress syndrome (ARDS) [4–7]. Adhesive interaction mediated by VE-cadherin (VE-cad) is primarily responsible for maintenance of the endothelial adherens junctions [8–11]. Several other adherens junctional proteins and molecular mediators play a role in maintaining the intact

✉ Kostandin V. Pajcini
kvp@uic.edu

[1] Department of Pharmacology and Regenerative Medicine, University of Illinois at Chicago College of Medicine, Chicago, IL 60612, USA

[2] Department of Biochemistry, University of Illinois at Chicago College of Medicine, Chicago, IL, USA

[3] Department of Physiology and Biophysics, University of Illinois College of Medicine, Chicago, IL 60612, USA

Published online: 27 August 2024

pulmonary vascular barrier, including claudin [12–15], and integrins [16–19]. The molecular mechanisms that regulate homeostatic and non-inflammatory processing of junctional proteins as well as delivery of VE-cadherin to the cell surface for resealing of the EC barrier remain largely unknown.

Notch signaling is a highly evolutionarily conserved metazoan signaling pathway. The expression patterns of Notch ligand Dll4 and the Notch1 receptor determine the fate of tip and stalk cells during angiogenesis [20, 21], as well as artery and venous specification [22]. While the role of Notch signaling in endothelial development [23], angiogenesis [24–26], and vascular cell fate decisions [22, 27] has been well established, the functional role of the Notch pathway in the homeostatic maintenance of the vascular barrier has only recently been explored. By primarily employing an in vitro microfluidic platform that relies on engineered microvessels, Polacheck et al. concluded that a non-canonical Notch signaling mechanism is responsible for adherens assembly, and that the Notch1 transmembrane domain regulates the vascular barrier function independent of transcriptional activation [28]. Since this compelling study, several others have investigated the role of Notch signaling components in EC barrier function under the context of LPS-mediated inflammatory in an in vitro transwell model system [29] and in an in vivo LPS induced sepsis model [30]. In both studies, transcriptional Notch pathway activation is seen in ECs in response to LPS treatment.

Canonical Notch activation proceeds through ligand interaction and successive proteolytic cleavages that release the intracellular domain (ICD) of Notch receptors. The ICD translocates to the nucleus and drives transcriptional activation of target genes through the formation of a tri-molecular complex with the DNA-binding protein RBPJκ and the co-factor MAML [31, 32]. Non-canonical Notch signaling has been observed in both invertebrate and vertebrate systems [33], however, its relevance is most prominently studied in the context of cancer where ligand-independent activation is associated with T-cell leukemia and a variety of other tumors [34–36]. Two Notch receptors, Notch1 and Notch4, are expressed on ECs during vascular development, and continue to be expressed in post-natal pulmonary ECs [37]. Despite being involved in multiple endothelial processes during development and angiogenesis, the role of canonical Notch signaling in establishing vascular adherens junctions is not clear and may not even be required. In this study, we utilized two in vivo, inducible, tissue specific ($CDH5Cre^{ERT2}$) transgenic murine models: (1) expression of the Dominant Negative Mastermind (DNMAML) [38, 39] and (2) deletion of the Notch1 receptor ($Notch1^{f/f}$) [40]. We set out to study how pan-inhibition of Notch transcriptional activity via DNMAML compares to loss of the Notch1 receptor with respect to lung EC barrier function in vivo. We demonstrate that Notch transcriptional signaling is essential to maintain pulmonary vascular integrity, in part, by a newly discovered, endothelial-specific Notch target: tmtc1. We show that tmtc1 interacts with and is important for export of VE-cadherin to the cell surface which we conclude is an important step to maintain a stable endothelial barrier.

Results

Tissue specific transcriptional inhibition of Notch signaling in endothelial cells disrupts pulmonary vascular integrity

To determine the role of Notch signaling in vascular permeability, we employed two transgenic murine model systems that specifically delete the Notch1 receptor, $Notch1^{f/f}$ or inhibit all canonical Notch transcriptional signaling via DNMAML in ECs by using the VE-Cadherin-specific Cre driver ($CDH5Cre^{ERT2}$) (Fig. 1A). The tissue specific expression of DNMAML does not affect the expression of Notch1 and Notch4 receptors. However, this system prevents the functional formation of the tri-molecular transcriptional complex with RBPJk and MAML with both Notch1 or Notch4 ICD and thus prevents transcriptional signaling [38, 39] without perturbing the expression of Notch1 and its transmembrane domain. Endothelial cells were isolated by FACS-sorting from lung tissue of each model system. FACS with surface markers $CD45^{-}$ $CD31^{+}$ indicate comparable numbers of CD31+ ECs isolated among mutants and WT lung cells (Fig. 1B). Disruption of Notch signaling was confirmed by measuring the mRNA expression of canonical Notch targets Hes1, Hey1, and EphrinB2 (Fig. 1C). DNMAML mutants and WT littermates show abundant Notch1 and Notch4 protein expression (Fig. 1D), indicating the presence of the receptors, but an inhibition of Notch transcriptional activation in sorted lung ECs (Fig. 1C). Furthermore, active/cleaved Notch1 protein expression is dramatically decreased in lung ECs harvested from $VEcadherinCre^{ERT2+}$ ($CDH5Cre^{ERT2+}$) $Notch1^{f/f}$ mice (Fig. 1D, E), while Notch4 and VE-cadherin protein expression is not significantly disrupted in either model (Fig. 1D, E).

Next, we assessed lung permeability in vivo via Evan's blue albumin assay (EBA) and capillary filtration coefficient (Kfc) to determine the extravasation of albumin and water through the lung vascular endothelial barrier, respectively. Both DNMAML and $Notch1^{f/f}$ exhibited an increase in extravasation of albumin (Fig. 2A) and of water (Fig. 2C). The wet/dry ratio was likewise increased in the lungs of DNMAML and $Notch1^{f/f}$ compared to the WT (Fig. 2B). We also analyzed the lung sections by H&E (Fig. 2D) in our murine models. The Notch mutant models exhibited lung endothelium characterized by an increase in the hyaline

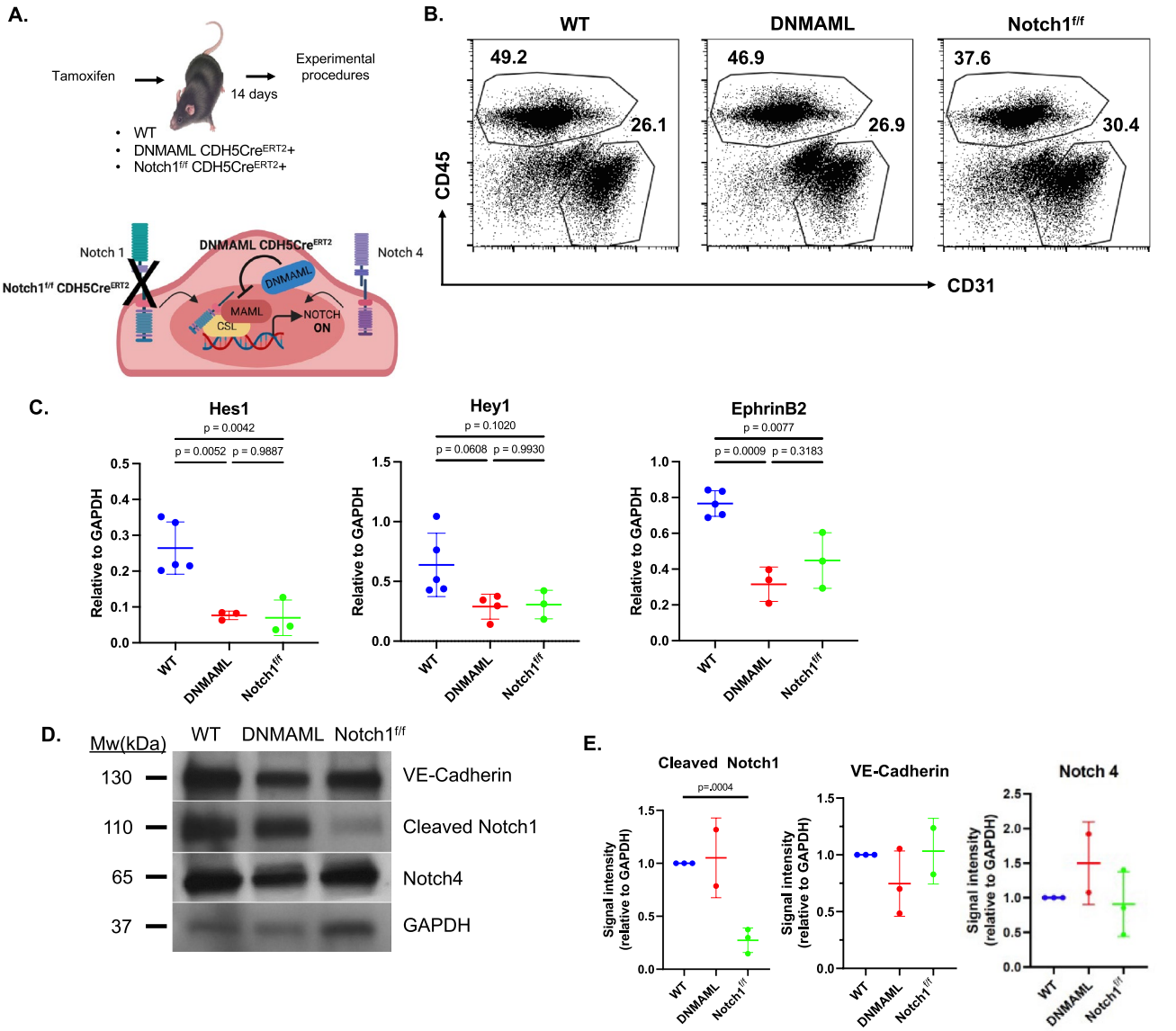

Fig. 1 Comparative inducible transgenic model systems for in vivo tissue specific inhibition of Notch pathway in lung endothelial cells (ECs). **A** (Top) experimental design of WT, DNMAML CDH5Cre^{ERT2} (DNMAML), Notch1$^{f/f}$ CDH5Cre^{ERT2} (Notch1$^{f/f}$) mice, and (bottom) illustration of the mechanism of pathway inhibition for each mutant model. Mice were injected with tamoxifen for 5 consecutive days to induce Cre activity in CDH5+endothelial cells. Mice were rested for 2-weeks before used for experiments. **B** Representative gating strategy for FACS-purified ECs in tamoxifen-treated WT, DNMAML and Notch1$^{f/f}$ mice. Cells were sorted for DAPI^{-} CD45^{-} CD31^{+}. **C** mRNA expression of canonical Notch targets Hes1, Hey1, and EphrinB2 in WT, DNMAML, and Notch1$^{f/f}$ mice. Hes1: *n* (individual mouse replicates)=5, 3, and 3 from left to right for each genotype. Hey1: *n* (individual mouse replicates)=5, 4, and 3 for each genotype. Ephrin B2: *n* (individual mouse replicates)=5, 3, and 3 for each genotype. Statistical analysis: one-way ANOVA. **D** Representative Western blot of cleaved-Notch1, Notch4, and VE-Cadherin in FACS-sorted lung ECs. GAPDH was used as a loading control. **E** Quantification of Western blot protein levels for cleaved-Notch1: *n* (individual mouse replicates) = 3, 2, 3 for each genotype. VE-Cadherin: *n* (individual mouse replicates) = 3, 3, 2 or each genotype. Notch4: *n* (individual mouse replicates) = 3, 2, 3 for each genotype

membrane thickness, debris filling the airspaces, and alveolar septal thickening (Fig. 2D, right panels) compared to that of the WT lungs [41, 42]. Considering these findings, we sought to determine the proliferation and the apoptosis status of the ECs in the lungs of the mutant mice. We analyzed sections from WT, DNMAML, and Notch1$^{f/f}$ lungs and observed an increase in the Ki67 staining (Fig. 2E top panels) but no difference in apoptosis as determined by Caspase-3 staining (Fig. 2E, bottom panels). Quantification of Ki67 staining shows significant more proliferation in the Notch1$^{f/f}$ lung sections compared to WT (Fig. 2E, right panels). Flow cytometric analysis of digested lungs of

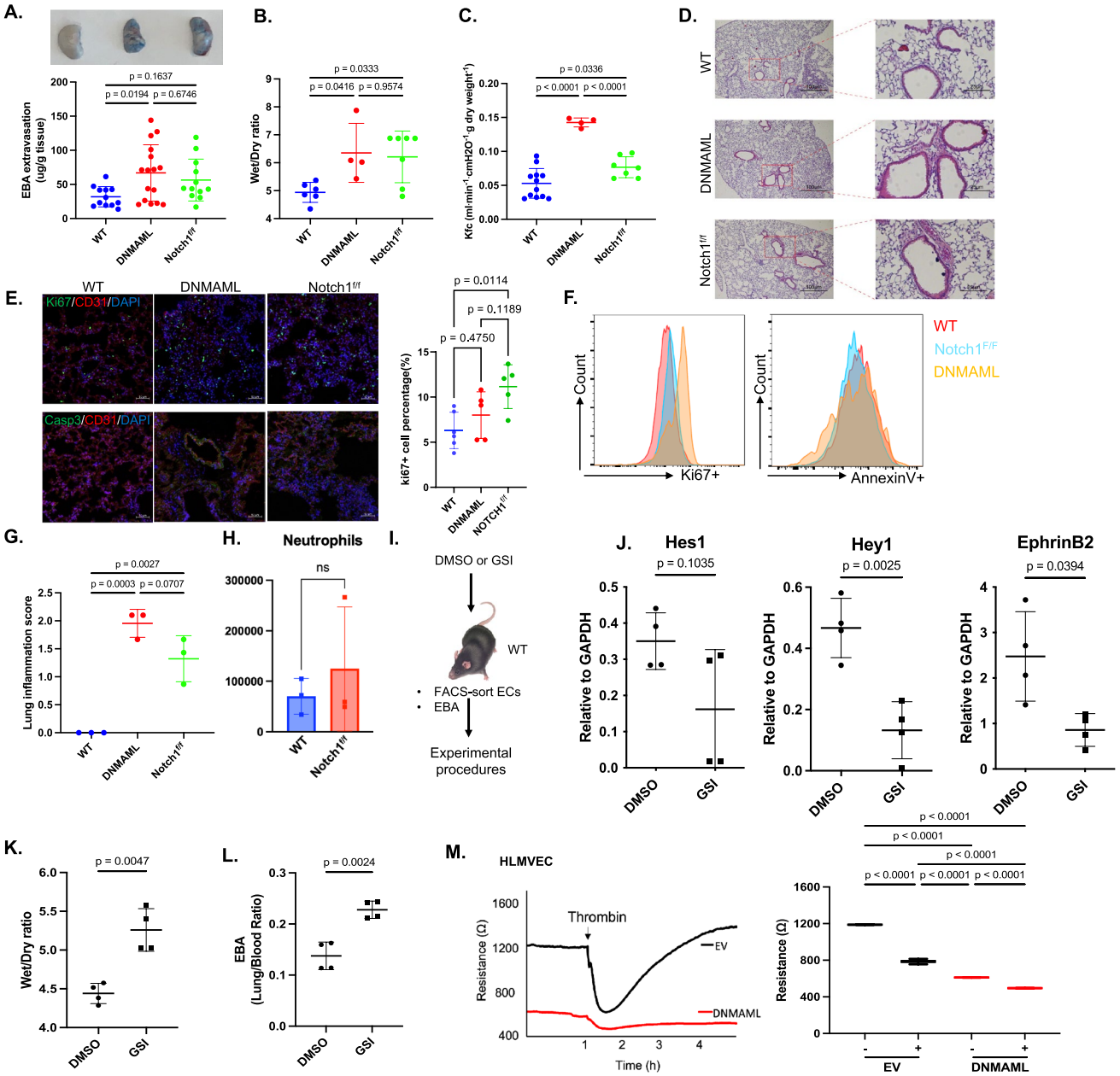

each model system, gated on CD45$^-$ CD31$^+$ shows a similar trend for Ki67 staining in Notch mutants, but no difference in pro-apoptotic status as determined by AnnexinV staining (Fig. 2F). Thus overall, DNMAML and Notch1$^{f/f}$ lung endothelium showed higher proliferation potential and a higher lung inflammation score (Fig. 2G).

We also analyzed the overall infiltration of granulocytes (CD45$^+$CD11b$^+$Gr1$^+$) in the WT or Notch1$^{f/f}$ lungs and our results indicate that a modest but non-significant increase in granulocyte numbers is seen in the Notch mutant lungs (Fig. 2H). These findings show that transcriptional inhibition of Notch signaling by DNMAML in vivo has a more severe defect in disrupting the vascular EC barrier than loss of the Notch1 receptor alone. Since inducible transgenic model systems require days for Cre activation and subsequent Notch pathway inhibition, to confirm these results in an expedient timeframe, we assessed whether vascular permeability is increased in a model of acute inhibition of Notch signaling via a small molecule gamma secretase inhibitor (GSI) [43, 44]. We treated WT mice for 16 h with DMSO (control) or GSI (Fig. 2I). The efficacy of GSI inhibition of Notch signaling was validated by assessing the mRNA expression of Hes1, Hey1, and EphrinB2 in FACS-sorted lung ECs (Fig. 2J). The wet/dry ratio and EBA extravasation

◂**Fig. 2** Loss of Notch signaling disrupts pulmonary vascular integrity and inhibition of Notch signaling increases vascular permeability. **A** (Top) Representative images and (bottom) quantification of EBA extravasation in perfused lungs. *n* (individual mouse replicates) = 12, 16, 12 from left to right for each genotype. Statistical analysis: one-way ANOVA. **B** Wet to dry ratio of lungs. *n* (individual mouse replicates) = 6, 4, 7 for each genotype. Statistical analysis: one-way ANOVA. **C** Capillary filtration coefficient (Kfc) in lungs. *n* (individual mouse replicates) = 12, 4, 7 for each genotype. Statistical analysis: one-way ANOVA. **D** H&E staining of section of WT, DNMAML, and Notch1$^{f/f}$ lungs. **E** IF staining of lung sections of WT, DNMAML and Notch1 for Ki67 (top) and cleaved Caspase3 (bottom). scale bar 50um. Quantification of Ki67 positive cells (%) in indicated genotypes (right). Statistical analysis: one-way ANOVA. **F** Representative flow cytometry histogram of ECs in tamoxifen-treated WT, DNMAML and Notch1$^{f/f}$ mice gated for DAPI$^-$ CD45$^-$ CD31$^+$ and analyzed for Ki67 (left) and AnnexinV (right). **G** Quantification of lung inflammation score. *n* (individual mouse replicates) = 3 for all conditions. Statistical analysis: one-way ANOVA. **H** Absolute granulocyte (CD45$^+$ CD31$^-$ CD11b$^+$ Gr1$^+$) numbers in WT and Notch1$^{f/f}$ lungs. *n* (individual mouse replicates) = 3. Statistical analysis: Welch's t-test. **I** Experimental design. WT mice were injected with 2 consecutive injections of DMSO or GSI (10 mg/kg total). Lungs ECs were FACS-purified for further experiments. **J** mRNA expression of Notch targets Hes1, Hey1, and EphrinB2 in FACS-sorted lung ECs from DMSO- or GSI-treated mice. Expression was normalized to GAPDH. *n* (individual mouse replicates) = 4 for both conditions. Statistical analysis: Welch's t-test. **K** Wet/Dry ratio. *n* (individual mouse replicates) = 4 for both conditions. Statistical analysis: Welch's t-test. **L** EBA extravasation of perfused lungs. *n* (individual mouse replicates) = 4 for both conditions. Statistical analysis: Welch's t-test. **M** (left) TEER of HLMVECs transfected with empty vector (EV) or DNMAML-encoding plasmids. Resistance was measured 48 h post-transfection. *n* (biological replicates) = 3 and 4. (right) quantification *n* (biological replicates) = 3, 3, 4, 4 from left to right. Statistical analysis: one-way ANOVA. Scale bar for D and E 100 µm and 25 µm, respectively

of the lungs were increased in GSI-treated mice compared to the DMSO-treated mice (Fig. 2K, L) which supported the results from the genetic models.

To determine if this loss of EC barrier integrity occurred due to inhibition of transcriptional Notch activity, we measured transendothelial electrical resistance (TEER) in human microvascular lung endothelial cells (HLMVECs) transfected with an empty vector (EV) or DNMAML construct and challenged with thrombin to induce a transient decrease of electrical resistance as a control (Fig. 2M). TEER reflects EC permeability based on combined adhesion of EC to adjacent EC and the extracellular matrix [45]. We found that DNMAML severely disrupted EC barrier function, consistent with our findings in vivo. We also challenged these cells with thrombin, which rapidly disrupts EC barrier function in a reversible manner [45, 46]. As expected, thrombin-induced a transient decrease in electrical resistance in control ECs, but DNMAML-treated cells had a significantly lower resistance at baseline and after thrombin treatment these cells failed to recover, indicating irreversible EC permeability after transcriptional Notch pathway inhibition (Fig. 2M). These findings suggest that disruption of canonical Notch signaling is required to maintain tight endothelial barrier function, and consequently results in increased vascular permeability.

Tmtc1 is a novel Notch transcriptional target required for maintenance of EC junctions

To determine which downstream Notch target gene(s) regulate the maintenance of vascular integrity in lung ECs, we sorted ECs from WT, DNMAML, and Notch1$^{f/f}$ lungs 2 weeks post-tamoxifen induction and assessed their transcriptional profiles by RNAseq. We identified several differentially expressed genes between DNMAML and Notch1$^{f/f}$ (Fig. 3A, B), of which, 24 genes were downregulated in both DNMAML and Notch1$^{f/f}$ cells when compared to WT control expression levels (Fig. 3D). In agreement with previous findings (see Fig. 2E, F), we observed an enrichment for S-phase genes in the Notch mutants when compared to WT (Fig. 3C). We initially assessed both slc6a2 and tmtc1 both of which were downregulated when Notch signaling was inhibited. Solute Carrier Family 6 Member 2 (slc6a2) is a norepinephrine transporter [47] and its expression in lung ECs was upregulated compared to heart ECs and brain ECs [48]. Liu et al. have shown it is downregulated in seawater aspiration-induced ALI [49], however, its mechanism in vascular permeability is unknown. Transmembrane *O*-Mannosyltransferase Targeting Cadherins 1 (tmtc1), is found in the endoplasmic reticulum [50], is required for the *O*-mannosylation of cadherins and protocadherins and acts as a transmembrane *O*-mannosyltransferase [51, 52].

We narrowed down our list of Notch targets by reanalyzing the Notch and RBPJ binding sites from a published ChIP-Seq dataset from HUVECs [53]. We identified tmtc1 as a putative downstream target gene as it contained predicted and functional DNA binding sites conserved for both Notch and RBPJ occupancy, while slc6a2 did not contain any Notch and RBPJ binding sites as determined by ChIP-Seq (Fig. 3E). To validate our transcriptomics analysis, we confirmed that tmtc1 mRNA (Fig. 3F) and protein expression (Fig. 3G, H) in ECs from DNMAML and Notch1$^{f/f}$ mice were significantly downregulated compared to the WT mice. To further validate whether tmtc1 is a Notch downstream target in HLMVECs, the cells were treated with GSI. Tmtc1 expression was markedly reduced, along with our positive control Hes1, a canonical Notch target [54]. Removal of GSI by washout then replaced with fresh media, similarly, restored the expression of Hes1 and tmtc1 (Fig. 3I). To confirm the regulatory site where the Notch complex binds and drives tmtc1 expression, HLMVECs were treated with either DMSO or GSI and chromatin immunoprecipitation (ChiP) with cleaved Notch1 antibody was performed. We specifically targeted the predicted 5′ promoter region of TMTC1. Our results show enriched binding of Notch1 in

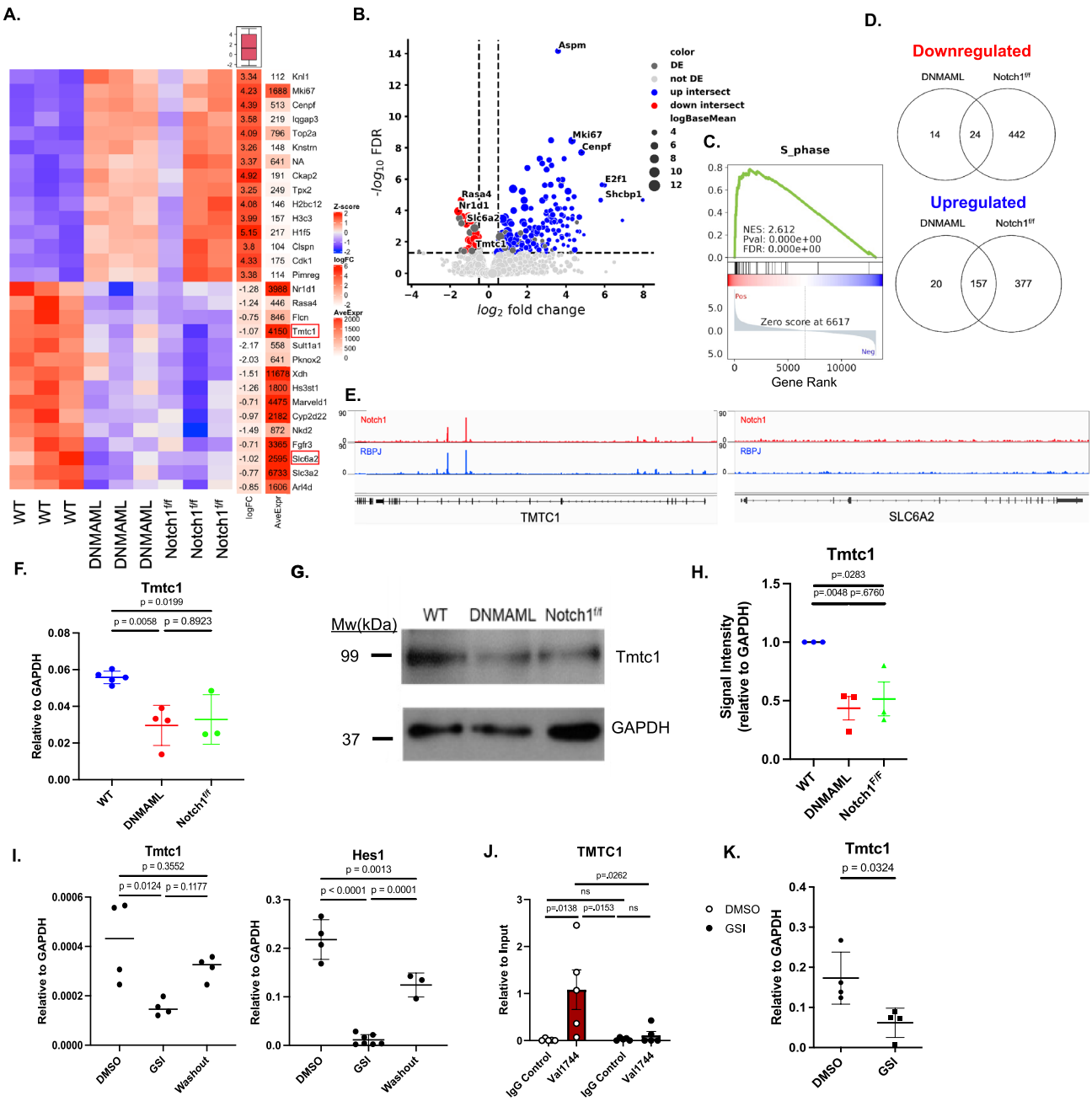

Fig. 3 Tmtc1 is a novel Notch transcriptional target in lung ECs. **A** Heat map of WT, DNMAML, and Notch1$^{f/f}$ lung bulk RNA-sequencing of sorted lung EC gene expression. Heat map shows the 15 highest upregulated and downregulated genes for each genotype. *n* (individual mouse replicates) = 3 for all conditions. **B** Volcano plot from RNAseq data of WT, DNMAML, and Notch1$^{f/f}$. **C** Enrichment plot for S phase genes in DNMAML lung ECs. **D** Venn diagram of DNMAML and Notch1$^{f/f}$ showing number of genes that were (top) downregulated or (down) upregulated from both RNAseq datasets compared to WT. **E** Representative Notch1 and RBPJ predicted regulatory binding regions identified by ChIP-seq for tmtc1 (top) and slc6a2 (bottom) in HUVECs. **F** Tmtc1 mRNA expression of FACS-sorted lung endothelial cells from mutant mice. Expression was normalized to GAPDH. *n* (individual mouse replicates) = 4, 4, and 3. Statistical analysis: one-way ANOVA. **G** Representative Western blot of Tmtc1. **H** Quantification of western blot of FACS-sorted lung ECs from WT, DNMAML, and Notch1$^{f/f}$ mice. GAPDH was used as a loading control. *n* (mouse biological replicates) = 3. Statistical analysis one-way ANOVA. **I** (left) Tmtc1 and (right) Hes1 mRNA expression of HLMVECs treated with DMSO, GSI, and 4-h washout. Expression was normalized to GAPDH. *n* (biological replicates) = 4, 4, and 3. Statistical analysis: one-way ANOVA. **J** Chromatin Immunoprecipitation of the TMTC1 promoter using Notch1 Val1744 antibody in HLMVECs treated with DMSO or GSI. *n* (technical replicates) = 5. **J** (left) Tmtc1 and (right) Hes1 mRNA expression of HLMVECs treated with DMSO, GSI, and 4-h washout. Expression was normalized to GAPDH. *n* (biological replicates) = 4, 4, and 3. Statistical analysis: one-way ANOVA. **K** Tmtc1 mRNA expression of WT mice treated with DMSO or GSI. Expression was normalized relative to GAPDH. *n* (individual mouse replicates) = 4 for both conditions. Statistical analysis: Welch's t-test

the control (DMSO) Notch-active cells when compared to the GSI-treated, Notch-inactive cells (Fig. 3J). Our findings were consistent in vivo as seen in WT mice treated with GSI, which show a downregulation of tmtc1 expression (Fig. 3K) in purified lung ECs. Along with the formation of the Notch transcriptional complex as indicated by ChIP-seq and local ChiP, our results indicate that tmtc1 is a direct downstream target gene of canonical Notch signaling.

Knockdown of tmtc1 leads to disruption of endothelial barrier function

Tmtc proteins are predicted to be a cadherin targeting proteins with specific function in post-translational modification of cadherins [51] and regulation of cellular adhesion [55]. We hypothesized that tmtc1 is essential for regulating junctional proteins in lung ECs. VE-Cadherin has been established as a key junctional protein in maintaining intact vascular barrier functions in the lung [10]. Several previous studies have shown that the internalization of VE-Cadherin from the plasma membrane leads to an increase in vascular permeability [10, 16]. To test the effect of tmtc1 suppression on EC barrier resistance, we performed TEER on HLMVECs that were transfected with scramble siRNA (siSc) or tmtc1 siRNA (siTmtc1) for 48 h, where ideal knockdown was confirmed and persisted until 72 h after initial treatment (Fig. 4A). By TEER measurement, Tmtc1 depleted ECs showed significantly lower resistance and disruption of barrier junctions than control siSc-treated cells (Fig. 4B). To visualize how the barrier could be affected by loss to tmtc1, we imaged cells by immunofluorescence after they were treated with siSc or siTmtc1 for 48 h to observe the condition of the tight junctions in HLMVECs. Our results show decreased localization of VE-Cadherin at junctions between

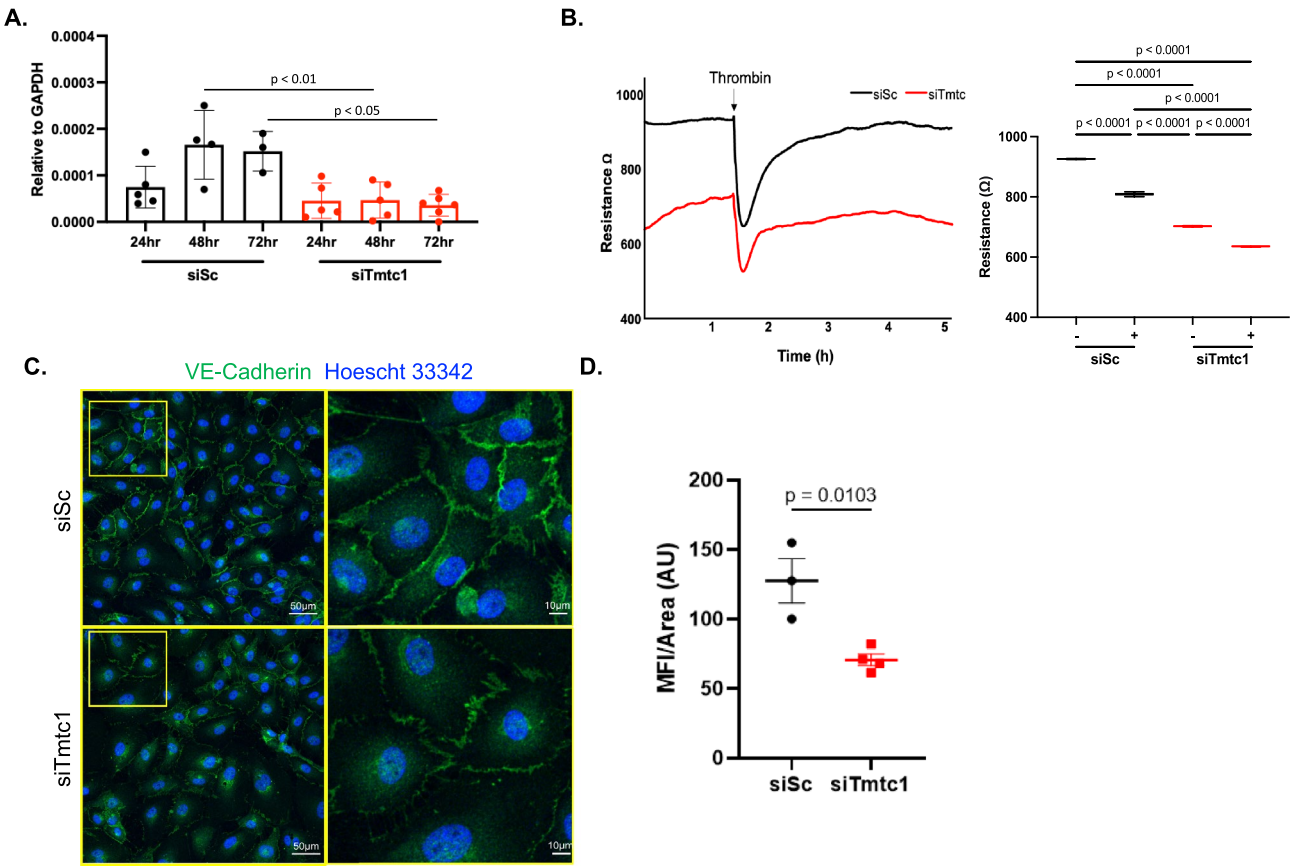

Fig. 4 Loss of tmtc1 negatively impacts endothelial junctional integrity. **A** Tmtc1 mRNA expression of HLMVECs transfected with siRNA Scrambled (siSc) or siTmtc1 at 24 h, 48 h, and 72 h. Expression was normalized relative to GAPDH. *n* (biological replicates) = 5, 4, 3, 5, 5 and 6. from left to right. Statistical analysis: one-way ANOVA. **B** (left) TEER of control siRNA (siSc) or tmtc1 siRNA treated cells (siTmtc1) and (right) quantification of TEER. *n* (biological replicates) = 3 for all conditions. Statistical analysis: one-way ANOVA. **C** Immunofluorescent staining of siSc- and siTmtc1-treated HLMVECs and **D** Quantification of junctional VE-Cadherin of siSc- and siTmtc1-treated HLMVECs *n* (biological replicates) = 3 and 4, respectively. Quantification determined by averaging VE-cadherin junctional fluorescent intensity per field of view. Statistical analysis: Welch's t-test. Cells were stained with VE-Cadherin (green) and Hoechst 33342 (blue)

ECs in the siTmtc1-treated cells than in those treated with siSc (Fig. 4C). Quantification of mean fluorescence intensity at junction area show a significant decrease of VE-Cadherin after tmtc1 knockdown (Fig. 4D). These results indicate that tmtc1 is essential in regulating endothelial tight junctions and suggest that it does so by regulating plasma membrane levels of VE-cadherin.

Loss of tmtc1 leads to the accumulation of VE-cadherin in the endoplasmic reticulum

To investigate the mechanism behind the disruption of barrier integrity resulting from the loss of tmtc1, we visualized VE-cadherin localization in control or tmtc1-depleted HLMVECs. The cells were transfected with siSc, siTmtc1 as well as empty vector (EV), or DNMAML. 48 h after treatment, the cells were fixed and stained and visualized by confocal microscopy for localization of endoplasmic reticulum (ER) marker SERCA2, VE-cadherin and nuclear marker DAPI (Fig. 5A). We found that that the loss of tmtc1, via direct siRNA treatment or by impairing Notch transcriptional signaling inhibition (DNMAML), led to the accumulation of VE-Cadherin in the ER of HLMVECs as denoted by colocalization of VE-Cadherin with SERCA2 (Fig. 5A, B). Loss of tmtc1 also decreased cell adhesion and cell spreading (Fig. 5A, 2nd and 4th rows). This suggested to us that the post-translational processing of VE-cadherin is perturbed when tmtc1 levels are decreased. To determine if plasma membrane expression of VE-cadherin is directly dependent on tmtc1, we performed a rescue experiment in HLMVECs. Cells were transfected with EV, DNMAML, or DNMAML+TMTC1 (Fig. 5C). 48 h after treatment all three groups were analyzed via flow cytometry for surface expression of VE-cadherin (Fig. 5D). Our findings, show that overexpression of tTmtc1 is sufficient to restore plasma membrane levels of VE-Cadherin after inhibition of Notch signaling (Fig. 5D, right panel). To determine whether the accumulation of VE-cadherin in the ER directly resulted from the loss of tmtc1 interaction, we performed co-immunoprecipitation in HLMVECs treated with siSc, siTmtc1, or DNMAML (Fig. 5E). Our results indicate that VE-cadherin binds with tmtc1 and that the loss of tmtc1, either via direct siRNA treatment or by Notch inhibition with DNMAML, decreases levels of its interaction with VE-cadherin. These findings suggest that loss of tmtc1 prevents the egress of VE-cadherin from the ER and thus hinders junctional integrity between ECs. To determine if accumulation VE-cadherin in the ER directly resulted from the loss of tmtc1 interaction, we performed co-immunoprecipitation in HLMVECs treated with siSc, siTmtc1, or DNMAML (Fig. 5E). Our results indicate that VE-cadherin binds with tmtc1 and that the loss of tmtc1, either via direct siRNA treatment or by Notch inhibition with DNMAML, decreases levels of its interaction with VE-cadherin. These findings suggest that loss of tmtc1 prevents the egress of VE-cadherin from the ER and thus hinders junctional integrity between ECs.

Discussion

The maintenance of a tight vascular endothelial barrier in the lungs is critical for proper gas exchange. Failure to maintain the barrier integrity leads to an influx of fluids, proteins, and cells into the lungs, causing edema, which is a hallmark of ALI/ARDS [4, 5, 7]. Thus, systemic disruption of endothelial junctions can lead to organ failure by dysregulation of vascular permeability and compromised tissue perfusion.

Many previous studies have shown Notch signaling to be critical for establishment of the vascular endothelial barrier during development [56, 57] and in the context of inflammatory responses [29, 30]. In each case, the role of Notch has been associated with initiation of receptor activation and downstream target gene regulation. More recent studies have proposed alternative models of Notch receptor function. In one recent study, ECs barrier junctions of becomes leaky due to the absence of the transmembrane domain of the Notch1 receptor [28]. In this study, Polacheck et al. proposed that the Notch receptor served a structural role for cell adhesion and VE-cadherin interaction. They further concluded that the effects of the Notch1 receptor in EC junctions did not involve transcription but that the transmembrane domain of Notch1 anchored both VE-cadherin and cytoskeletal components which are required for EC barrier maintenance. A similar, structural, non-canonical, role for the Notch1 receptor was recently shown to regulate epithelial adherens junctions and cortical actin organization using an in vitro microfluidic platform of ductal epithelium [58]. Non-canonical activation of Notch receptor has also been previously reported in arterial endothelial ECs [59] where high shear stress can produce the biophysical force necessary for receptor cleavage [60]. Though receptor activation is mediated in ECs encountering high shear stress, once the Notch1 receptor is cleaved by non-canonical means, the downstream signaling mechanism is based on activation of transcriptional target genes [59]. Thus, the structural roles proposed by Polacheck et al. and White et al. fully decouple the evolutionary conserved transcriptional apparatus from the functional outcome of Notch signaling. The above-mentioned studies advanced our understanding of how the structural components of Notch receptors can regulate adherens junctions; still, the question whether canonically regulated Notch target genes can account for loss of adherens junctions during endothelial homeostasis has remained elusive, especially since no direct Notch target gene has been shown to be a structural component of the endothelial junctions.

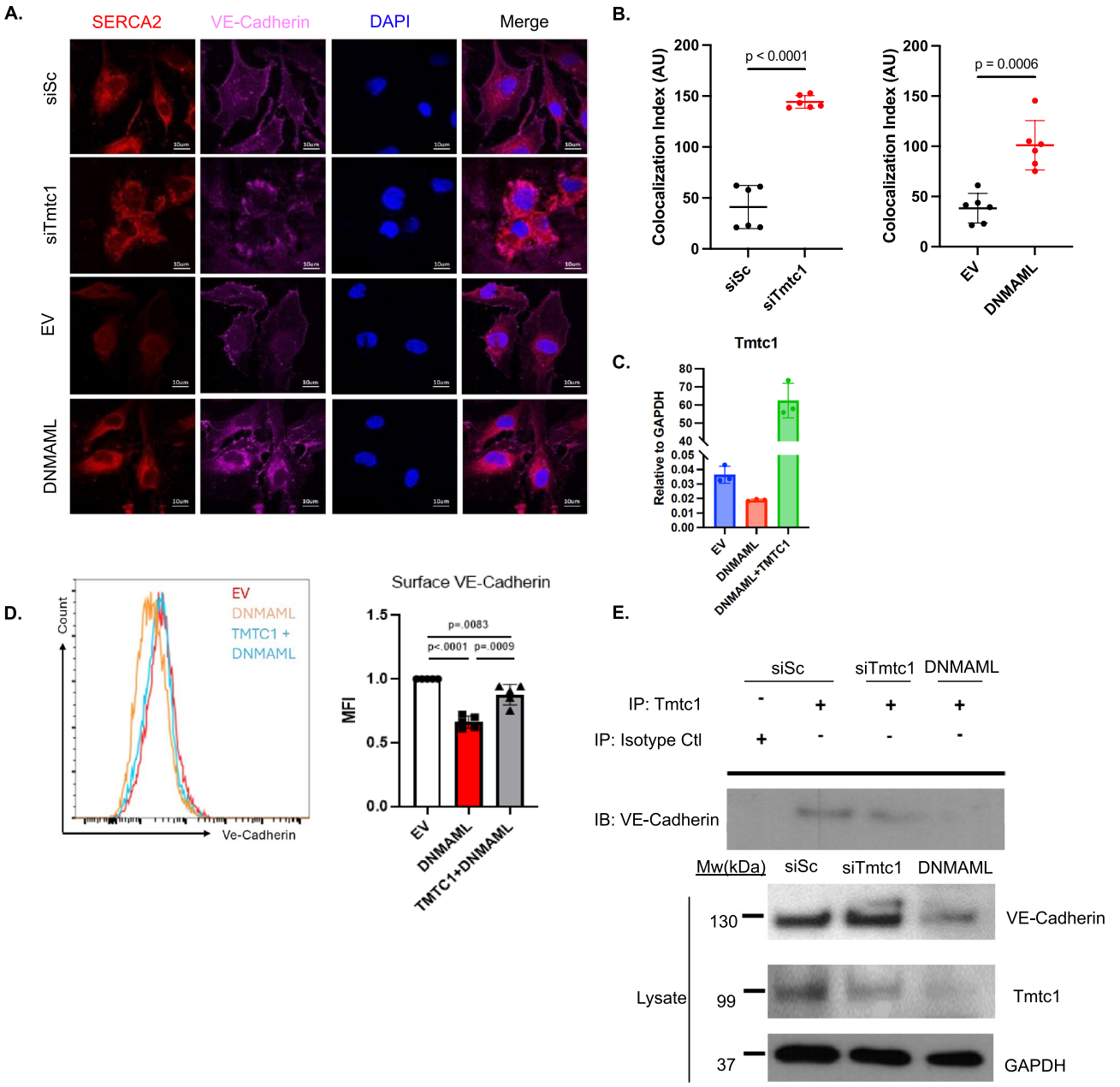

Fig. 5 Accumulation of VE-Cadherin in the endoplasmic reticulum after tmtc1 knockdown. **A** Immunofluorescent imaging of siSc-, siTmtc1-, EV-, and DNMAML-treated HLMVECs. Cells were stained with SERCA2 (red), VE-Cadherin (magenta) and DAPI (blue). **B** Quantification of colocalization of SERCA2 and VE-Cadherin from (left) siSc- and siTmtc1-, and (right) EV- and DNMAML-treated HLMVECs is represented by individual experiments. *n* (biological replicates) = 6 for all conditions. Statistical analysis: Welch's t-test. **C** RT-qPCR of Tmtc1 in EV, DNMAML, and DNMAML+TMTC1 transfected HLMVECs, *n* (technical replicates) = 3. **D** Surface VE-Cadherin expression detected by flow cytometry of HLMVECs transfected with EV, DNMAML, or DNMAML+TMTC1. *n* (biological replicates) = 5 for all conditions. Statistical analysis one-way ANOVA. **E** (Top) Co-Immunoprecipitation analysis of Tmtc1 and VE-Cadherin. HLMVECs were transfected with siSc, siTmtc1, and DNMAML. The cell lysates were immunoprecipitated with anti-Tmtc1 and were probed for VE-Cadherin. Representative (bottom) loading Western blot lysate for VE-Cadherin, Tmtc1, and GAPDH from total HLMVECs transfected with siSc, siTmtc1, and DNMAML. *n* (biological replicates) = 2

In our study, we have set out to initially compare the structural and transcriptional effects of Notch pathway inhibition in vivo, and then to discover new putative transcriptional target genes that can account for the role of Notch signaling in maintaining intact endothelial barrier junctions. Our in vivo lung EC analysis revealed a clear and pronounced

deficiency in EC barrier maintenance, with increased albumin and water extravasation as well as lung edema when pan-transcriptional inhibition was induced by tissue specific expression of DNMAML. We reasoned this surpasses the effect of Notch1 deletion since DNMAML inhibits transcriptional activation of the intracellular domains of both Notch1 and Notch4, both of which are abundantly expressed receptors in lung endothelial cells. Through unbiased bulk RNA sequencing of lung ECs in each transgenic model system we discovered many putative gene targets that were both upregulated and downregulated. Initially, we focused on downregulated genes that were detected in both transgenic model systems, reasoning that loss of function to a critical gene in both model systems would be an ideal candidate to pursue in further studies of EC barrier maintenance. However, our findings also show that loss of Notch signaling stimulates a strong proliferative response in lung ECs. To determine target genes, we required independent identification of Notch complex formation in predicted RBPJ-bound regulatory regions of target genes. We did this by using a previously published ChIp-Seq dataset on HUVECs [53], and we further confirmed this result by performing local ChIP on HLMVECs. Though several promising target genes were initially investigated, only tmtc1 matched both qualifying criteria, and it is why other genes downregulated in both DNMAML and Notch1 lung ECs, such as Fgfr3 and slc6a2, were not pursued further.

Tmtc1 is part of the tmtc family of proteins: tmtc1-4 [50, 51]. Tmtc proteins have been shown to play various roles in glycosylation of the cadherin/protocadherin family of proteins. Previous studies have shown the knockout of all tmtc genes (tmtc1-4) in HEK293 cells downregulated the *O*-mannosylation of E-cadherin [52]. Furthermore, GWAS study has identified tmtc1 as a gene essential for lung function [61], but its specific role in endothelial barrier function has yet to been studied. Since tmtc1 is found in the ER [50], we determined from our in vitro imaging analysis and immunoprecipitation that loss of tmtc1 protein levels, by direct knockdown or by DNMAML-mediated Notch inhibition, prevents proper egress of VE-Cadherin in the ER. From these observations, we hypothesized that this leads to a failure of quality control for VE-cadherin protein therefore restricting it from the cell surface where it is required to exert its role in maintaining barrier integrity [10, 15]. Considering that the tmtc1 family of protein is involved in multiple post-translational modifications ranging from glycosylation to *O*-mannosylation, we acknowledge that our current study cannot fully establish how tmtc1 post-translationally modifies VE-cadherin. However, we do show that reintroduction of ectopic tmtc1 in a DNMAML-expressing lung endothelial cells rescues VE-cadherin protein surface levels. Thus, tmtc1, a novel transcriptional Notch target is essential for proper trafficking of VE-Cadherin to the plasma membrane and maintenance of endothelial barrier integrity. Though further studies are required, including a tmtc1 inducible transgenic model system to validate its specific role in vivo in the lung barrier vascular permeability, our study has identified a mechanistic process that is responsible for maintenance of vascular integrity in the pulmonary endothelial cells.

Materials and methods

Mice

Transgenic mice DNMAML (Jackson Laboratory, 032613) and Notch1$^{f/f}$ (Jackson Laboratory; 006951) were crossed with CDH5Cre^{ERT2}, provided by Dr. Ralf Adams (Max Planck Institute), to either inhibit Notch signaling transcription or delete Notch1 receptor specifically in endothelial cells. To induce transgene expression, mice were injected in intraperitoneally at 4 weeks of age with tamoxifen (Sigma-Aldrich), 75 mg/kg dissolved in corn oil (Sigma-Aldrich) for 5 consecutive days and left to recover for 2 weeks before experimental procedures. Cre-negative littermates were used as controls. For in vivo GSI experiments, C57BL/6 mice (The Jackson Laboratory; 000664) were injected with two consecutive doses of 10 mg/kg of GSI intraperitoneally. Mice were used for experiments 16 h after the last injection. All mice used in the studies were of C57BL/6J background and had access to food and water ad libitum. Both male and female mice in equal proportion were used for our studies. The Institutional Animal Care and Use Committees of UIC approved all experimental procedures used in this study.

Evan's blue albumin

Six-week-old mice were injected with Evans blue dye (10 mg/ml in PBS; 100 µl) (Sigma-Aldrich) retro-orbitally. Twenty minutes post-injection, mice were anesthetized with ketamine (100 mg/kg) and xylazine (15 mg/kg) and rested for 10 min. Lungs were perfused with 3 ml of PBS and harvested. Freeze-dried lung samples were weighed and incubated with 500 µl formamide at 56 °C, followed by centrifugation. Optical density was measured at 620 nm (EB) and 740 nm (heme).

Capillary coefficient Kfc

Mice were anesthetized with 2.5% isoflurane using a nose cone and injected with heparin (100 IU). The mouse lung was isolated, arterioles were cannulated, and perfused via a peristaltic pump. The lungs were perfused at a rate of 2 ml/min, and the venous pressure was increased from 2 to 12 mmHg for 10 min. The arterial and venous pressures as

well as the lung wet weight were recorded throughout the experiment. Kfc values were calculated by comparing the lung weight gain during the hydrostatic pressure change, and the filtration rate was normalized by the microvascular pressure change and the lung dry weight.

FACS-sorting of lung endothelial cells

Lungs were harvested from mice immediately after euthanasia with 5% isoflurane, followed by cervical dislocation. The tissue was cut into smaller pieces and digested with 0.1% collagenase A (Sigma-Aldrich) into PBS containing 2% fetal bovine serum (Gibco) for 45 min at 37 °C on a shaker. During the digestion step, cells were dispersed using a 18-gauge needle (BD Biosciences) and syringe (BD Biosciences). Cells were prepared into single cell suspension by gently passing through a 70 µm cell strainer (CellTreat). Red blood cells were lysed with ACK Lysing Buffer (Gibco).

Once in single cell suspension, cells were incubated with Dynabeads sheep anti-rat IgG (Invitrogen) that was conjugated to rat anti-mouse CD45 antibody (Biolegend) for 1 h at 4 °C on a shaker. Magnetic sorting was then used to separate the CD45+ and CD45- (supernatant) cells. Supernatant was collected and the cells bound to the magnet were washed twice with PBS containing 2% fetal bovine serum. Cells were centrifuged and resuspended with PBS containing 2% fetal bovine serum. Cells were stained with CD45.2 (Biolegend; Clone 104) and CD31 (Biolegend; Clone 390) at 1:200 dilution for 30 min. DAPI was used as a live/dead cell stain. DAPI- CD45- CD31+ cells were sorted via MoFlo Astrios (Beckman Coulter). FACS-sorted cells were used for qPCR, Western Blot, and RNAseq experiments.

qRT-PCR

Primary mouse lung endothelial cells and primary human microvascular lung endothelial cells (Lonza) were isolated for RNA using RNeasy Mini Kit (Qiagen). cDNA was synthesized from RNA with Super Script III synthesis kit (Invitrogen). SYBR Green (Applied Biosystems) was used, and qRT-PCR was performed on the Viia7 instrument (Applied Biosystems). GAPDH or EF1α were used as controls. Mouse primer sequences are as followed: GAPDH (5′-AACTTTGGCATTGTGGAAGG-3′; 5′-GGATGCAGGGATGATGTTCT-3′), Ef1a (5′-CACTTGGTCGCTTTGCTGTT-3′; 5′-GGTGGCAGGTGTTAGGGGTA-3′), Hes1 (5′-GAAAGATAGCTCCCGGCATT-3′; 5′-GTCACCTCGTTCATGCACTC-3′), Hey1 (5′-GGTACCCAGTGCCTTTGAGA-3′; 5′-ACCCCAAACTCCGATAGTCC-3′), EphrinB2 (5′-GTGAAGCCAAATCCAGGTTCTA-3′; 5′-ATGCGATCCCTGCGAATAAG-3′), Notch1 (5′-CTGTCCTCTGCCATATACAGGAGC-3′; 5′-ACCTCGCAGGTTTGACCTTGCCAG-3′), VE-Cadherin (5′-ACGAACTGGATTCTCGGGGTAACC-3′; 5′-ATCTGTACTACCAGCTTGCCCTGG-3′) and Tmtc1 (5′-AGAACAGCAAGGCTGAAGAG-3′; 5′-TGTCGGCCAGTGTTGTAATAG-3′). Human primer sequences are as followed: GAPDH (5′-CAGCCTCAAGATCATCAGCA-3′; 5′-TGTGGTCATGAGTCCTTCCA-3′), Hes1 (5′-GAAAGATAGCTCCCGGCATT-3′; 5′-GTCACCTCGTTCATGCACTC-3′), and Tmtc1 (5′-ATATGGGACATGCGGAACTTAG-3′; CCTTGTGCTCCAGTCTCTTAAA-3′).

Cell lysates and immunoblots

Whole cell lysates were prepared with RIPA buffer (Sigma Aldrich) with Halt Protease Inhibitor Cocktail (ThermoFisher Scientific). Protein concentration was determined with DC Protein Assay (Biorad). For immunoprecipitation, whole cell lysates were prepared and incubated with 1 µg specific antibody overnight at 4 °C. This was followed by incubation with Protein A Agarose beads (20 µl; Cell Signaling Technology) for 2 h at 4 °C. The beads were washed five times and analyzed by SDS–polyacrylamide gel electrophoresis (SDS–PAGE). Lysates and immunoprecipitates resolved by SDS–PAGE were transferred with transfer buffer (30 mM Tris, 250 mM Glycine, 1 mM EDTA, 20% methanol) to PVDF membranes (Millipore Sigma) at 4 °C for 2 h at 100 V. Membranes were blocked with 5% non-fat milk in 0.1% TBST (10 mM Tris–HCl pH 8.0, 150 mM NaCl, 0.1% Tween-20) at room temperature for 1 h. After washing, the membrane was incubated with primary antibodies overnight at 4 °C. After washing, the membrane was incubated with secondary-HRP-conjugated antibody for 1 h at room temperature. The membranes were developed using Super Signal Western blot detection reagents (Thermo Fisher Scientific) and signals were detected by X-ray film.

The following antibodies have been used: Cleaved Notch1 Val1744 (Cell Signaling), Anti-VE-Cadherin (Santa Cruz), Anti-Notch4 (Millipore Sigma), Anti-Tmtc1 (Proteintech), GADPH (Invitrogen). The following secondary antibodies were used: Goat Anti-Rabbit IgG-HRP Conjugate (Biorad), Goat Anti-Mouse IgG-HRP Conjugate (Biorad), Goat Anti-Rabbit IgG-HRP Conjugate (Biorad). Blots were developed with SuperSignal West Femto Maximum Sensitivity Substrate (Thermo Fisher Scientific). Signal intensity of bands was quantified using ImageJ.

Cell culture

Human microvascular lung endothelial cells (HLMVECs) were cultured in EGM-2 medium (Lonza) and used for in vitro GSI (γ-secretase inhibitor) siRNA transfection, and Western blot experiments. Confluent well of HLMVECs were treated with DMSO (Sigma-Aldrich) or GSI (1 µm) (Cayman Chemical) for 16 h before a 4 h washout experiment. Cells were harvested at the end of the experiment

for RNA isolation and qRT-PCR experiments. For siRNA transfections, cells at 80% confluency were transfected with negative siRNA (L-016838-01-0005; Horizon Discovery Dharmacon) or tmtc1 siRNA (D-001810-01-05; Horizon Discovery Dharmacon) using siRNA transfection reagent (Santa Cruz) and siRNA transfection medium (Santa Cruz). Cells were harvested 24-, 48-, and 72-h post-transfection for RNA isolation and qRT-PCR experiments. Human primer sequences are listed above in the Methods section for qPCR. For Western blots, cells at 80% confluency were transfected with negative siRNA, tmtc1 siRNA, as described, or MigR1-DNMAML using Fugene transfection reagent (Promega). Cells were harvested 48-h post-transfection for Western blot analysis. For the rescue experiment, cells at 90% confluency were transfected with MigR1-Empty Vector (EV), -DNMAML, or TMTC1 plasmids. After 48 h, cells were harvested with Accutase (ThermoFisher), washed with full EGM-2 medium, and rested on ice for 30 min. Cells were stained with anti-VE-cadherin (Biolegend) for 30 min and washed with DAPI in 2% FBS/PBS with calcium and magnesium added. Cells were analyzed via flow cytometry on the CytoFLEX S Flow Cytometer.

TEER

HLMVECs were seeded on 8-well gold-plated electrodes (Applied Biosciences), and cells were transfected with either plasmids (MigR1-EV or MigR1-DNMAML) for 72 h or with siRNAs (tmtc1 and scramble) for 96 h. Post-transfection at the mentioned time points, cells were serum starved for 1–2 h, and basal TEER was measured, followed by stimulation with 50 nM thrombin[53]. Note: For siRNA transfections, cells were transfected twice at a gap of 48 h time duration.

Immunofluorescent staining

We harvested the lungs of mice and froze the tissues into cryoblocks. Lung tissues were sectioned into 7 mm thick sections. Slides were fixed with 4% PFA for 10 min at room temperature, then blocked by 5% donkey serum and 0.5% Triton X-100 at room temperature for 1 h. We Incubated the slides with primary antibodies Ki67 (CST: #9129T), cleaved caspase 3 (CST: # 9664S) overnight at 4 °C. After washing, the slides were incubated with secondary antibody for 1 h at room temperature followed by DAPI staining. Images were captured by Zeiss LSM880 confocal microscopy.

HLMVECs were seeded on a 6-well glass bottom plate and transfected with either siRNAs (tmtc1 or scramble) or MigR1-EV or MigR1-DNMAML plasmids. Forty-eight hours post-transfection, cells were fixed with neutral buffered 10% formalin solution for 4 h, followed by 3 washes with PBS with calcium and magnesium. Cells were then permeabilized with 0.5% Triton-X-100 + donkey serum in PBS for 2 h at room temperature, followed by 3 PBS washes. Cells were incubated with VE-Cadherin antibody (1:50; Santa Cruz) and AlexaFluor 633 Phalloidin (1:1000; Invitrogen), and Hoechst 33342 (1:1000) or VE-Cadherin antibody (1:50; Santa Cruz), and SERCA2 ATPase antibody (1:100, Invitrogen), and DAPI (1:1000). For antibody incubation, 0.1% Triton-X-100 supplemented with 2% donkey serum in PBS was used. Cells were then mounted with ProLong Glass Antifade Mountant (ThermoFisher), prior to imaging. Images were analyzed using ImageJ to quantify colocalization index and junctional VE-Cadherin. Briefly, for analysis of cell surface expression of VE-Cadherin, multiple regions of interest of the same size were drawn on the plasma membrane, and pixel intensity was calculated. Intensity obtained from multiple regions of interest from the same image was averaged. Each *n* corresponds to the average of individual images. Colocalization between VE-Cadherin and SERCA2 ATPase was quantified using the Colocalization Threshold plugin of ImageJ.

Chromatin immunoprecipitation (ChIP) assay

ChIP analysis was performed using EZ-ChIP assay kit (Millipore, Billerica, MA, 17-295) according to the instruction from the manufacturer. Briefly, DMSO- and GSI-treated HLMVECs were crosslinked with 4% formaldehyde for 15 min at room temperature. Nuclear extracts were sonicated to produce 200–1000 bp DNA fragments. Chromatin-protein complexes were immunoprecipitated with anti-Notch1 Val1744 antibody or rabbit normal IgG. DNA was purified and the RT-qPCR reaction was performed with TMTC1 primers (5′-AGGTGGGTGTGGGGGTTCCAGA-3′ 5′-AAC GAACGTCCACCTGGCCCCAA-3′).

RNAseq

Total RNA was extracted via Qiagen RNeasy Plus Kit (Qiagen), DNAse treated, and purified using an RNA Clean & Concentrator MagBead with DNase I Included kit (Zymo Research). RNA samples were quantified for RNA and DNA content using a Qubit fluorometer (Invitrogen) and analyzed for integrity using Agilent 4200 TapeStation. Levels of remaining DNA did not exceed 10% of the total amount of nucleic acid.

Sequencing libraries for Illumina sequencing was prepared in one batch in a 96-well plate using CORALL Total RNA-seq Library Prep Kit with Unique Dual Indices with RiboCop HMRv2 rRNA Depletion (Lexogen).

In brief, approximately 20–30 nanograms of total RNA per sample were used for the first rRNA depletion step, then followed by library generation initiated with random oligonucleotide primer hybridization and reverse transcription.

Next, the 3′ ends of first-strand cDNA fragments were ligated with a linker containing Illumina-compatible P5 sequences and Unique Molecular Identifiers (UMIs). During the following steps of second strand cDNA synthesis and ds cDNA amplification, i7 and i5 indices as well as complete adapter sequences required for cluster generation were added. The number of PCR amplification cycles was 14 as determined by qPCR using a small pre-amplification library aliquot for each individual sample.

Final amplified libraries were purified, quantified, and average fragment sizes were confirmed to be approximately 350 bp by gel electrophoresis using 4200 TapeStation and D5000 Screen Tape (Agilent). The concentration of the final library pool was confirmed by qPCR and the pool was subjected to test sequencing on MiniSeq instrument (Illumina) to check sequencing efficiencies and adjust accordingly proportions of individual libraries. Sequencing was carried out on NovaSeq 6000 (Illumina), S4 flowcell, 2/150 bp, and 60 paired-end reads per sample performed at the Roy J. Carver Biotechnology Center at the University of Illinois at Urbana-Champaign. The data has been deposited to the NCBI Gene Expression Omnibus (GEO) database (Accession Number: GSE245264).

Statistics

Statistical analysis was performed using GraphPad Prism. Values were presented as mean with ± SD. Comparison of variables between 2 groups was calculated using Welch's t-test. Comparison of > 2 groups were calculated using a one-way ANOVA. The level of significance was set at a p value of < 0.05.

Acknowledgements We thank Paulina Rodriguez who helped maintain the murine colonies and performed genotyping. We would also to thank Dr. Balaji Ganesh and Dr. Wei Feng from the Flow Cytometry Core at UIC for providing instrumental resources. Dr. Jiwang Chen and Ayman Istaban from the Cardiovascular Research Core, and Dr. Zarema Arbieva Genomic Research Core at UIC provided data in this article.

Author contributions NYP designed and performed the experiments and wrote the manuscript. JN, MA, PG, MS, JH performed experiments. JWS, JR, and DM contributed to experimental design and manuscript review. KVP designed the experiments and wrote the manuscript.

Funding This study was supported by National Heart, Lung, and Blood Institute (Grant No. R01HL134971), (Grant No. R01HL151720) to KVP.

Data availability The RNA sequencing data has been deposited to the NCBI Gene Expression Omnibus (GEO) database (Accession Number: GSE245264). All other primary data is available upon request.

Declarations

Competing interests The authors declare no competing interests exist.

Ethical approval This study was performed in line with the principles of the Declaration of Helsinki. The Institutional Animal Care and Use Committees of UIC approved all experimental procedures used in this study. IACUC IBC approval 21-090.

Consent to publish We consent for open access publication of our article in Cellular and Molecular Life Sciences, Springer Nature.

References

1. Komarova Y, Malik AB (2010) Regulation of endothelial permeability via paracellular and transcellular transport pathways. Annu Rev Physiol 72:463–493
2. Tornavaca O, Chia M, Dufton N, Almagro LO, Conway DE, Randi AM, Schwartz MA, Matter K, Balda MS (2015) ZO-1 controls endothelial adherens junctions, cell-cell tension, angiogenesis, and barrier formation. J Cell Biol 208:821–838
3. Tsukita S, Furuse M, Itoh M (2001) Multifunctional strands in tight junctions. Nat Rev Mol Cell Biol 2:285–293
4. Dushianthan A, Grocott MP, Postle AD, Cusack R (2011) Acute respiratory distress syndrome and acute lung injury. Postgrad Med J 87:612–622
5. Rubenfeld GD (2003) Epidemiology of acute lung injury. Crit Care Med 31:S276–S284
6. Rubenfeld GD, Caldwell E, Peabody E, Weaver J, Martin DP, Neff M, Stern EJ, Hudson LD (2005) Incidence and outcomes of acute lung injury. N Engl J Med 353:1685–1693
7. Ware LB, Matthay MA (2000) The acute respiratory distress syndrome. N Engl J Med 342:1334–1349
8. Andresen Eguiluz RC, Kaylan KB, Underhill GH, Leckband DE (2017) Substrate stiffness and VE-cadherin mechano-transduction coordinate to regulate endothelial monolayer integrity. Biomaterials 140:45–57
9. Campinho P, Vilfan A, Vermot J (2020) Blood flow forces in shaping the vascular system: a focus on endothelial cell behavior. Front Physiol 11:552
10. Dejana E, Vestweber D (2013) The role of VE-cadherin in vascular morphogenesis and permeability control. Prog Mol Biol Transl Sci 116:119–144
11. Lai Y, Huang Y (2021) Mechanisms of mechanical force induced pulmonary vascular endothelial hyperpermeability. Front Physiol 12:714064
12. Kakogiannos N, Ferrari L, Giampietro C, Scalise AA, Maderna C, Rava M, Taddei A, Lampugnani MG, Pisati F, Malinverno M, Martini E, Costa I, Lupia M, Cavallaro U, Beznoussenko GV, Mironov AA, Fernandes B, Rudini N, Dejana E, Giannotta

M (2020) JAM-A acts via C/EBP-alpha to promote claudin-5 expression and enhance endothelial barrier function. Circ Res 127:1056–1073
13. Li X, Li R, Fang Q, Jamal M, Wang C, Wang Y, Zhang Z, Wu X, Song X (2021) Oxycodone attenuates vascular leak and lung inflammation in a clinically relevant two-hit rat model of acute lung injury. Cytokine 138:155346
14. Morita K, Sasaki H, Furuse M, Tsukita S (1999) Endothelial claudin: claudin-5/TMVCF constitutes tight junction strands in endothelial cells. J Cell Biol 147:185–194
15. Wang T, Gross C, Desai AA, Zemskov E, Wu X, Garcia AN, Jacobson JR, Yuan JX, Garcia JG, Black SM (2017) Endothelial cell signaling and ventilator-induced lung injury: molecular mechanisms, genomic analyses, and therapeutic targets. Am J Physiol Lung Cell Mol Physiol 312:L452–L476
16. Alghisi GC, Ponsonnet L, Ruegg C (2009) The integrin antagonist cilengitide activates alphaVbeta3, disrupts VE-cadherin localization at cell junctions and enhances permeability in endothelial cells. PLoS ONE 4:e4449
17. Hakanpaa L, Kiss EA, Jacquemet G, Miinalainen I, Lerche M, Guzman C, Mervaala E, Eklund L, Ivaska J, Saharinen P (2018) Targeting beta1-integrin inhibits vascular leakage in endotoxemia. Proc Natl Acad Sci USA 115:E6467–E6476
18. Su G, Hodnett M, Wu N, Atakilit A, Kosinski C, Godzich M, Huang XZ, Kim JK, Frank JA, Matthay MA, Sheppard D, Pittet JF (2007) Integrin alphavbeta5 regulates lung vascular permeability and pulmonary endothelial barrier function. Am J Respir Cell Mol Biol 36:377–386
19. Yamamoto H, Ehling M, Kato K, Kanai K, van Lessen M, Frye M, Zeuschner D, Nakayama M, Vestweber D, Adams RH (2015) Integrin beta1 controls VE-cadherin localization and blood vessel stability. Nat Commun 6:6429
20. Blanco R, Gerhardt H (2013) VEGF and Notch in tip and stalk cell selection. Cold Spring Harb Perspect Med 3:a006569
21. Hellstrom M, Phng LK, Hofmann JJ, Wallgard E, Coultas L, Lindblom P, Alva J, Nilsson AK, Karlsson L, Gaiano N, Yoon K, Rossant J, Iruela-Arispe ML, Kalen M, Gerhardt H, Betsholtz C (2007) Dll4 signalling through Notch1 regulates formation of tip cells during angiogenesis. Nature 445:776–780
22. Swift MR, Weinstein BM (2009) Arterial-venous specification during development. Circ Res 104:576–588
23. Lawson ND, Scheer N, Pham VN, Kim CH, Chitnis AB, Campos-Ortega JA, Weinstein BM (2001) Notch signaling is required for arterial-venous differentiation during embryonic vascular development. Development 128:3675–3683
24. Adams RH, Alitalo K (2007) Molecular regulation of angiogenesis and lymphangiogenesis. Nat Rev Mol Cell Biol 8:464–478
25. Benedito R, Roca C, Sorensen I, Adams S, Gossler A, Fruttiger M, Adams RH (2009) The notch ligands Dll4 and Jagged1 have opposing effects on angiogenesis. Cell 137:1124–1135
26. Limbourg FP, Takeshita K, Radtke F, Bronson RT, Chin MT, Liao JK (2005) Essential role of endothelial Notch1 in angiogenesis. Circulation 111:1826–1832
27. You LR, Lin FJ, Lee CT, DeMayo FJ, Tsai MJ, Tsai SY (2005) Suppression of Notch signalling by the COUP-TFII transcription factor regulates vein identity. Nature 435:98–104
28. Polacheck WJ, Kutys ML, Yang J, Eyckmans J, Wu Y, Vasavada H, Hirschi KK, Chen CS (2017) A non-canonical Notch complex regulates adherens junctions and vascular barrier function. Nature 552:258–262
29. Moll M, Reichel K, Nurjadi D, Former S, Krall LJ, Heeg K, Hildebrand D (2021) Notch ligand delta-like 1 is associated with loss of vascular endothelial barrier function. Front Physiol 12:766713
30. Liu T, Zhang C, Ying J, Wang Y, Yan G, Zhou Y, Lu G (2023) Inhibition of the intracellular domain of Notch1 results in vascular endothelial cell dysfunction in sepsis. Front Immunol 14:1134556
31. Kopan R, Ilagan MX (2009) The canonical Notch signaling pathway: unfolding the activation mechanism. Cell 137:216–233
32. Bray SJ (2006) Notch signalling: a simple pathway becomes complex. Nat Rev Mol Cell Biol 7:678–689
33. Ayaz F, Osborne BA (2014) Non-canonical notch signaling in cancer and immunity. Front Oncol 4:345
34. Lee KS, Wu Z, Song Y, Mitra SS, Feroze AH, Cheshier SH, Lu B (2013) Roles of PINK1, mTORC2, and mitochondria in preserving brain tumor-forming stem cells in a noncanonical Notch signaling pathway. Genes Dev 27:2642–2647
35. Pear WS, Aster JC (2004) T cell acute lymphoblastic leukemia/lymphoma: a human cancer commonly associated with aberrant NOTCH1 signaling. Curr Opin Hematol 11:426–433
36. Weng AP, Aster JC (2004) Multiple niches for Notch in cancer: context is everything. Curr Opin Genet Dev 14:48–54
37. Akil A, Gutierrez-Garcia AK, Guenter R, Rose JB, Beck AW, Chen H, Ren B (2021) Notch signaling in vascular endothelial cells, angiogenesis, and tumor progression: an update and prospective. Front Cell Dev Biol 9:642352
38. Tu L, Fang TC, Artis D, Shestova O, Pross SE, Maillard I, Pear WS (2005) Notch signaling is an important regulator of type 2 immunity. J Exp Med 202:1037–1042
39. Maillard I, Weng AP, Carpenter AC, Rodriguez CG, Sai H, Xu L, Allman D, Aster JC, Pear WS (2004) Mastermind critically regulates Notch-mediated lymphoid cell fate decisions. Blood 104:1696–1702
40. Yang X, Klein R, Tian X, Cheng HT, Kopan R, Shen J (2004) Notch activation induces apoptosis in neural progenitor cells through a p53-dependent pathway. Dev Biol 269:81–94
41. Matute-Bello G, Downey G, Moore BB, Groshong SD, Matthay MA, Slutsky AS, Kuebler WM, Acute Lung Injury in Animals Study Group (2011) An official American Thoracic Society workshop report: features and measurements of experimental acute lung injury in animals. Am J Respir Cell Mol Biol 44:725–738
42. Schmidt ME, Knudson CJ, Hartwig SM, Pewe LL, Meyerholz DK, Langlois RA, Harty JT, Varga SM (2018) Memory CD8 T cells mediate severe immunopathology following respiratory syncytial virus infection. PLoS Pathog 14:e1006810
43. Wolfe MS (2020) Unraveling the complexity of gamma-secretase. Semin Cell Dev Biol 105:3–11
44. De Strooper B, Annaert W, Cupers P, Saftig P, Craessaerts K, Mumm JS, Schroeter EH, Schrijvers V, Wolfe MS, Ray WJ, Goate A, Kopan R (1999) A presenilin-1-dependent gamma-secretase-like protease mediates release of Notch intracellular domain. Nature 398:518–522
45. Mehta D, Malik AB (2006) Signaling mechanisms regulating endothelial permeability. Physiol Rev 86:279–367
46. Ukropec JA, Hollinger MK, Salva SM, Woolkalis MJ (2000) SHP2 association with VE-cadherin complexes in human endothelial cells is regulated by thrombin. J Biol Chem 275:5983–5986
47. Bruss M, Kunz J, Lingen B, Bonisch H (1993) Chromosomal mapping of the human gene for the tricyclic antidepressant-sensitive noradrenaline transporter. Hum Genet 91:278–280
48. Jambusaria A, Hong Z, Zhang L, Srivastava S, Jana A, Toth PT, Dai Y, Malik AB, Rehman J (2020) Endothelial heterogeneity across distinct vascular beds during homeostasis and inflammation. eLife. 9:e51413. https://doi.org/10.7554/eLife.51413
49. Liu W, Pan L, Zhang M, Bo L, Li C, Liu Q, Wang L, Jin F (2016) Identification of distinct genes associated with seawater aspiration-induced acute lung injury by gene expression profile analysis. Mol Med Rep 14:3168–3178
50. Sunryd JC, Cheon B, Graham JB, Giorda KM, Fissore RA, Hebert DN (2014) TMTC1 and TMTC2 are novel endoplasmic reticulum

tetratricopeptide repeat-containing adapter proteins involved in calcium homeostasis. J Biol Chem 289:16085–16099
51. Eisenhaber B, Sinha S, Jadalanki CK, Shitov VA, Tan QW, Sirota FL, Eisenhaber F (2021) Conserved sequence motifs in human TMTC1, TMTC2, TMTC3, and TMTC4, new O-mannosyltransferases from the GT-C/PMT clan, are rationalized as ligand binding sites. Biol Direct 16:4
52. Larsen ISB, Narimatsu Y, Joshi HJ, Siukstaite L, Harrison OJ, Brasch J, Goodman KM, Hansen L, Shapiro L, Honig B, Vakhrushev SY, Clausen H, Halim A (2017) Discovery of an O-mannosylation pathway selectively serving cadherins and protocadherins. Proc Natl Acad Sci USA 114:11163–11168
53. Poulsen LC, Edelmann RJ, Kruger S, Dieguez-Hurtado R, Shah A, Stav-Noraas TE, Renzi A, Szymanska M, Wang J, Ehling M, Benedito R, Kasprzycka M, Baekkevold E, Sundnes O, Midwood KS, Scott H, Collas P, Siebel CW, Adams RH, Haraldsen G, Sundlisaeter E, Hol J (2018) Inhibition of endothelial NOTCH1 signaling attenuates inflammation by reducing cytokine-mediated histone acetylation at inflammatory enhancers. Arterioscler Thromb Vasc Biol 38:854–869
54. Iso T, Sartorelli V, Poizat C, Iezzi S, Wu HY, Chung G, Kedes L, Hamamori Y (2001) HERP, a novel heterodimer partner of HES/E(spl) in Notch signaling. Mol Cell Biol 21:6080–6089
55. Graham JB, Sunryd JC, Mathavan K, Weir E, Larsen ISB, Halim A, Clausen H, Cousin H, Alfandari D, Hebert DN (2020) Endoplasmic reticulum transmembrane protein TMTC3 contributes to O-mannosylation of E-cadherin, cellular adherence, and embryonic gastrulation. Mol Biol Cell 31:167–183
56. Scheppke L, Murphy EA, Zarpellon A, Hofmann JJ, Merkulova A, Shields DJ, Weis SM, Byzova TV, Ruggeri ZM, Iruela-Arispe ML, Cheresh DA (2012) Notch promotes vascular maturation by inducing integrin-mediated smooth muscle cell adhesion to the endothelial basement membrane. Blood 119:2149–2158
57. Shawber CJ, Das I, Francisco E, Kitajewski J (2003) Notch signaling in primary endothelial cells. Ann N Y Acad Sci 995:162–170
58. White MJ, Jacobs KA, Singh T, Mayo LN, Lin A, Chen CS, Jun YW, Kutys ML (2023) Notch1 cortical signaling regulates epithelial architecture and cell-cell adhesion. J Cell Biol. 222(12):e202303013. https://doi.org/10.1083/jcb.202303013
59. Mack JJ, Mosqueiro TS, Archer BJ, Jones WM, Sunshine H, Faas GC, Briot A, Aragon RL, Su T, Romay MC, McDonald AI, Kuo CH, Lizama CO, Lane TF, Zovein AC, Fang Y, Tarling EJ, de Aguiar Vallim TQ, Navab M, Fogelman AM, Bouchard LS, Iruela-Arispe ML (2017) NOTCH1 is a mechanosensor in adult arteries. Nat Commun 8:1620
60. Gordon WR, Zimmerman B, He L, Miles LJ, Huang J, Tiyanont K, McArthur DG, Aster JC, Perrimon N, Loparo JJ, Blacklow SC (2015) Mechanical allostery: evidence for a force requirement in the proteolytic activation of Notch. Dev Cell 33:729–736
61. Yao TC, Du G, Han L, Sun Y, Hu D, Yang JJ, Mathias R, Roth LA, Rafaels N, Thompson EE, Loisel DA, Anderson R, Eng C, Arruabarrena Orbegozo M, Young M, Klocksieben JM, Anderson E, Shanovich K, Lester LA, Williams LK, Barnes KC, Burchard EG, Nicolae DL, Abney M, Ober C (2014) Genome-wide association study of lung function phenotypes in a founder population. J Allergy Clin Immunol 133(248–255):e241–e210